ISSN 2007-9737

Automated Lung Segmentation on Computed Tomography Image for the Diagnosis of Lung Cancer

Ratishchandra Huidrom, Yambem Jina Chanu, Khumanthem Manglem Singh

National Institute of Technology, Department of Computer Science and Engineering, Manipur, India

{ratishchandra.huidrom, jina.yambem, manglem}@gmail.com

Abstract. Image processing techniques are widely used in several medical areas for early detection and treatment especially in the detection of various cancer tumors such as Squamous, Adenocarcinoma, Large Cell Carcinomas and Small Cell Lung Cancer. Segmentation of lung tissues from Computed Tomography (CT), image is considered as a pre-processing step in Lung Imaging. However, during Lung Segmentation, the Juxta-Pleural nodules (nodules attach to parenchymal walls), are missed out as they have similar appearance (intensity) to that of other non-pulmonary structures, which leads to a challenge to segment lung region along with Juxta-Pleural nodules. The complexity to segment lung region is mainly due to its inhomogeneity (different structures and intensity values of lungs). Thus, the existing segmentation algorithms like image thresholding algorithm, region-growing algorithm, active contour, level sets, etc. fail to segment lung tissues including Juxta-Pleural nodules. So, in this paper, a new fully-automated lung segmentation method with Juxta-Pleural nodules inclusion, is proposed.

Keywords. Computed tomography, image processing, juxta-pleural nodules, lung segmentation, image thresholding, lung imaging.

1 Introduction

Lung Cancer is one of the most serious fatal diseases. It is the leading cause of cancer death among both men and women. As per American Cancer Society's publication, Cancer Facts & Figures 2017 [1], about 155,870 deaths from lung cancer are estimated for the year of 2017 in the USA alone. The possibility of lung cancer is about 1 in every 13 men and about 1 in every 16 women. The treatment of lung cancer is effective only during its early stages.

The early detection of lung cancer can be performed effectively with the help of an automated cancer detection system.

Many researchers investigate the development of the computer-aided diagnosis (CAD), system for lung cancer from different image modalities. The performance of a particular CAD system can be evaluated in terms of accuracy, the number of false positives, speed, and automation level. The input of a CAD system is the medical images obtained from an appropriate modality. The segmentation of lung region is a pre-processing step of the CAD system in order to reduce the search space for the detection of lung nodules. In nodule detection step, the locations of lung nodules are detected. The detected nodules are then segmented. Finally, a candidate set of features such as appearance feature, shape and volume are extracted, and used for diagnosis [2].

Here, we focus only in lung segmentation on which the performance of the whole CAD system depends. It is the most critical step of CAD system as the remaining steps proceed on the segmented lung. The most common usage of lung segmentation algorithm is to quantify the lung disease progression, regression or stagnation and change in the visual extent of disease over time. It is also an important marker of response to therapy and a predictor for chances of survival. Lung segmentation algorithms are also commonly used as a pre-processing step for the segmentation of other lung structures and anomalies, such as nodules, vessels, lobules, and fissures.

In this paper, an automated lung segmentation method is proposed, which is used to segment lung region including Juxta-Pleural nodules.

The performance of the method is evaluated by using data available from the Lung Image Database Consortium (LIDC) [3], and data collected from Regional Institute of Medical Sciences, Imphal (RIMS). It is also compared with that of the existing Image Thresholding method [4], and then concluded that the proposed method yields better performance than the existing method.

The rest of the paper is organized as follows: Section 2, Related Works, a brief overview of the existing methods is presented. Section 3, Methodology, the proposed method for the segmentation of lung including Juxta-Pleural nodules is described. Section 4, Experimental Results and Analyses, the performance of the proposed method is evaluated and compared it with the performance of the existing Image Thresholding method. At the last section of this paper, the conclusion and future works are included.

2 Related Works

Hu *et al.* [4], practiced an Iterative Thresholding, Dynamic Programming, and Morphological operations. They achieved Root Mean Square Distance (RmsD), as 0.8 pixel. Mendonca *et al.* [5] showed the Sensitivity (Sen.) of 0.9225 and Positive Predictive Value (PPV), of 0.968 by using spatial edge detector method. Yim *et al.* [6] used both region growing and connected component labeling and showed Root Mean Square Distance (RmsD) of 1.2 pixel. Overlap Measure (OM), of 0.8165 has been shown by Sluimer *et al.* [7] using the shape-based method. Campadelli *et al.* [8] produced the value of Sensitivity (Sen.) of 0.9174, Specificity (Spec.) of 0.9584, Positive Predictive Value (PPV) of 0.9197 and Accuracy (Acc.) of 0.9437 by using spatial edge detector method. Korfiatis *et al.* [9], showed the value of Overlap Measure (OM) as 0.983 and Root Mean Square Distance (RmsD) as 0.52 mm by using wavelet edge detector method. Gao *et al.* [10] demonstrated the value of Dice Similarity Coefficient (DSC) as 0.9946 by using thresholding method. Shi *et al.* [11], studied the method of the shape-based deformable model with 0.92 Overlap Measure (OM).

Table 1. Summary of existing methods of lung segmentation

Model	Approach	Performance
Hu *et al.* [4]	Iterative Thresholding	RmsD = 0.8 pixel
Mendonca *et al.* [5]	Spatial Edge Detection	Sen = 0.9225 PPV = 0.968
Yim *et al.* [6]	Region Growing	RmsD = 1.2 pixel
Sluimer *et al.* [7]	Shape-based method	OM = 0.8165
Campadelli *et al.* [8]	Spatial Edge Model	Sen = 0.9174 Spec =0.9584
Korfiatis *et al.* [9]	Wavelet Edge Detection	OM = 0.983 RmsD=0.52mm
Gao *et al.* [10]	Thresholding	DSC = 0.9946
Shi *et al.* [11]	Shape-based Deformable Model	OM = 0.92
El-Baz *et al.* [12]	Statistical MGRF	Acc = 0.968
Annangi *et al.* [13]	Shape-based Deformable Model	DSC = 0.88
Kockelkorn *et al.* [14]	Statistical classification	OM = 0.96
Besbes *et al.* [15]	Shape-based Technique	OM = 0.9474
Hua *et al.* [16]	Graph search Technique	Sen = 0.986 Spec = 0.995
Sun *et al.* [17]	Active Shape Model	DSC = 0.975
Abdollahi *et al.* [18]	Statistical MGRF	DSC = 0.960

El-Baz *et al.* [12], practiced statistical MGRF model and found the value of Accuracy (Acc.) as 0.968.

Annangi *et al.* [13], worked the shape-based deformable model technique and gave the value of Dice Similarity Coefficient (DSC) as 0.88. Kockelkorn *et al.* [14] found the value of Overlap Measure (OM), as 0.96 by prior training and statistical classifier technique. Besbes *et al.* [15] used the shape-based technique and found the value of Overlap Measure (OM) as 0.9474. Hua *et al.* [16] reported the value of Sensitivity (Sen.) as

0.986 and Specificity (Spec.) as 0.995 by graph search technique. Sun *et al.* [17], used the shape-based technique and found the value of Dice Similarity Coefficient (DSC) as 0.975. Abdollahi *et al.* [18] worked the statistical MGRF model technique and showed the value of Dice Similarity Coefficient (DSC) as 0.960.

The existing Lung Segmentation methods focused on the accuracy of the segmentation but Juxta-Pleural nodule cases were not considered. A brief summary of the above mentioned existing methods of Lung Segmentation is given in Table 1.

3 Methodology

The goal of the lung segmentation is to separate the voxels corresponding to lung tissue from the voxels corresponding to the surrounding anatomy. In our proposed method, there are two steps to segment lung tissues from CT scan image, namely (i) Lung Field Extraction and (ii) Boundary Analysis and Segmentation of Lung. In the first step, extraction of the lung field is performed by using Image Thresholding technique and Connected Component Analysis. Here, the extracted lung field does not include Juxta-Pleural nodules. Most of the existing thresholding-based Lung Segmentation methods finalized in this Lung Field Extraction step, extended with some morphological smoothing post processing steps. The addition of the proposed method can be seen in the next processing step, it is designed to include Juxta-Pleural nodules in the Lung Segmentation.

In the second step, the boundaries of both left and right lungs are analyzed by identifying Juxta-Pleural nodules affecting lung boundaries, and then segment lung region with Juxta-Pleural nodule inclusion. Under the following subsections, the two steps of the proposed method are described in details.

3.1 Lung Field Extraction

Lung Field Extraction step is divided into three parts: (a) Background Suppression, (b) Lung Field Extraction by Thresholding, and (c) Lung Volume Extraction using Connected Component Analysis.

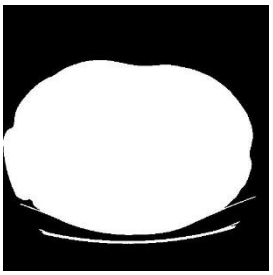

Fig. 1. Background Suppression

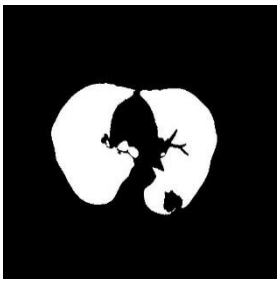

Fig. 2. Lung Field Extraction

First, the Background Suppression extracts the body region by removing the surrounding air space.

Then, the Lung Field Extraction by Thresholding separates the lung tissues from the extracted body but at this stage, Juxta-Pleural nodules cannot be included. Finally, the Lung Volume Extraction using Connected Component Analysis reconstructs 3D lung model of the lungs from the 2D slices of the extracted lung regions.

a. Background Suppression

The surrounding air space of the patient's body on CT scan image, is removed by using Image Thresholding technique with a threshold value of-600 H.U. Then, a morphological hole filling operation is applied on the thresholder image in order to include the lung inside the segmented body. Finally, each of pixel on the thresholder image is multiplied with the corresponding pixel on the original CT image, in order to get the body without the surrounding air space, as shown in Figure 1.

b. Lung Field Extraction by Thresholding

After background suppression, the background pixels are replaced with white pixels, so that the lung field which has lesser intensity, can be extracted easily. The extraction of lung field is performed by using Image Thresholding technique [19] with a threshold value of -500 H.U. But, the internal airways of lung are lighter in intensity compare to that of lung.

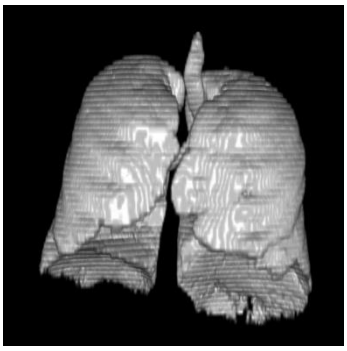

Fig. 3. 3D view of Extracted Lung Volume after applying Connected Component Analysis

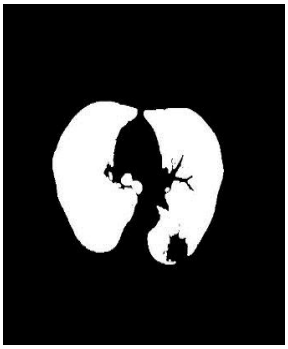

Fig. 4. Extracted Lung Field

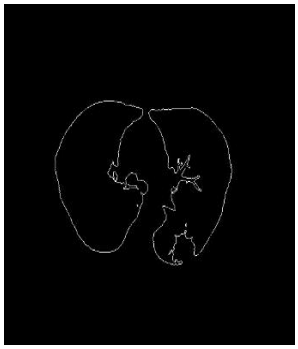

Fig. 5. Sobel Edge Detection

Hence, a morphological hole filling operation is applied to include all the airways inside the lung, as shown in Figure 2.

c. Lung Volume Extraction using Connected Component Analysis

In this step, the lung volume is extracted. There are other internal structures and organs which are of similar intensity to that of the lung. Those structures and organs are usually not attached to the lung, and hence they can also be removed by using 3D Connected Component Analysis [20], using 6-Neighborhood Connectivity.

Since both left and right lungs are connected with bronchi and both lungs occupy maximum volume in the thorax, lung volume is extracted by choosing the largest number of voxels among all the connected components, as shown in Figure 3.

3.2 Boundary Analysis and Segmentation of Lung

After lung field extraction, in this step, the boundary edges of the extracted lung field are analyzed in order to include Juxta-Pleural nodules. First, the edges of the extracted lungs from the binary lung field images are detected using Sobel Edge Detection Technique [21].

The lung images after applying Lung Field Extraction and Sobel Edge Detection are shown in Figure 4 and 5. In the following subsections, the polar coordinates of the edge points are detected from the detected edges of lungs, then Juxta-Pleural nodules are detected from the upper boundary edge points, and finally, the lung boundaries at Juxta-Pleural nodule locations are reconstructed.

a. Detection of Polar Coordinates of the Edge Points

After the detection of the lung edges, the edge points which is in Cartesian coordinate system are detected and then converted into Polar Coordinate System. First, the white edge pixels are extracted and the Cartesian coordinates of the extracted edge points are detected. The centroid of the edge points of the lung is considered as the origin of the coordinate system.

Then, the coordinates of the edge points are converted in Polar Coordinate System by using the following equations:

$$\theta = \tan^{-1}\left(\frac{y - y_0}{x - x_0}\right), \tag{1}$$

$$r = \sqrt{(x - x_0)^2 + (y - y_0)^2}\,, \tag{2}$$

where θ is the angle and r is the radial distance of the point (x, y) from the origin (x_0, y_0).

The extracted edge points in Cartesian Coordinate System is shown in Figure 6 with center as a red dot in the middle. After the conversion to Polar Coordinate System, the edge points are plotted in XY plane such that the angle (in degree) of the polar coordinates, is plotted

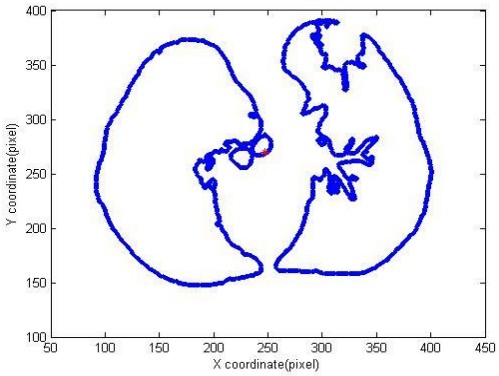

Fig. 6. Extracted Cartesian Points

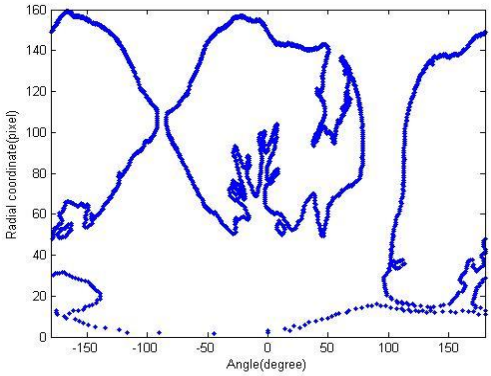

Fig. 7. Plotting Polar Coordinate Points on XY plane

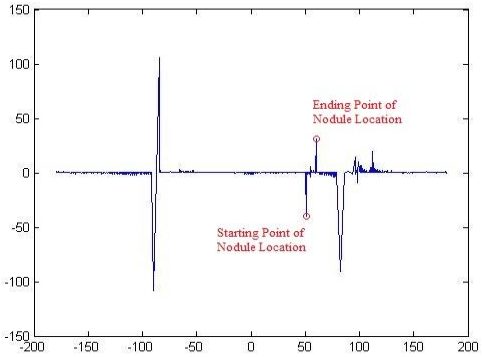

Fig. 8. Juxta-Pleural Nodule Detection from Derivative of lung boundary

along x-axis and the radial distance along y-axis, as shown in Figure 7.

b. Juxta-Pleural Nodule Detection

From the Figure 7, the upper boundary line is extracted using Max function. The derivative of this boundary line is then thresholded with two fixed threshold values T_{low} and T_{high}, derived from the value of CT Image resolution, on both positive and negative sides of the derivative. The peaks which lie between the two threshold values on both negative and positive sides, respectively mark the starting and ending points of Juxta-Pleural Nodules. Figure 8 shows the detection of the Juxta-Pleural nodule.

c. Boundary Reconstruction using Gray-level Profiling

From the above detected Juxta-Pleural nodule location, the boundary of the lung at Juxta-Pleural nodule location, is reconstructed by using Gray-level Profiling [21]. After Gray-level profiling the edge points are further aligned by using an 1D averaging filter. Figure 9 and 10 show the segmented lung before and after Gray-level Profiling.

Finally, the region of Juxta-Pleural nodule is filled by using morphological hole filling operation. The images of the lungs before and after the lung segmentation are shown below:

4. Experimental Results and Analyses

In order to evaluate the performance of the proposed system, we need ground-truth images which have to be compared with. We calculate true positive (TP), true negative (TN), false positive (FP) and false negative (FN) using logical pixel-wise operators as follows:

– **True Positive (TP):** True Object.

$$TP = GT \wedge SI \,. \tag{3}$$

– **True Negative (TN):** True Background.

$$TN = \neg\left(GT \vee SI\right). \tag{4}$$

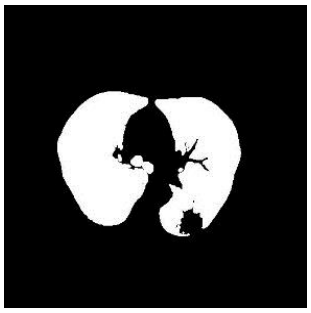

Fig. 9. Before Gray-level Profiling

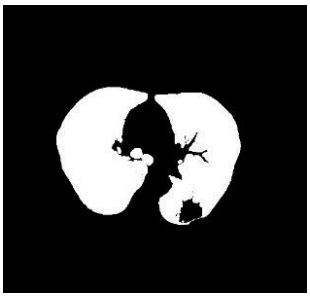

Fig. 10. After Gray-level Profiling

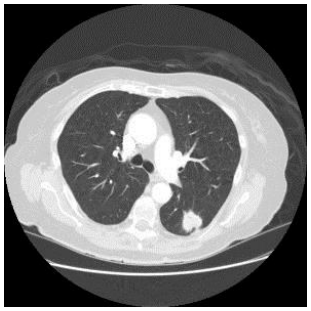

Fig. 11. Before Segmentation

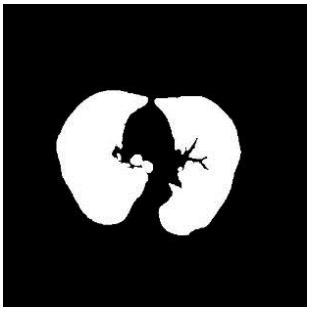

Fig. 12. After Segmentation

– **False Positive (FP):** A part of background region falsely segmented as a part of object.

$$FP = (GT \oplus SI) \wedge SI \,. \tag{5}$$

– **False Negative (FN):** A part of object region falsely segmented as a part of background:

$$FN = (GT \oplus SI) \wedge GT \,. \tag{6}$$

where GT is Ground Truth Image, SI is the Segmented Image, $\wedge$ is AND operator, $\vee$ is OR operator, $\neg$ is NOT operator and $\oplus$ is XOR operator.

From these values, we calculate seven performance parameters: Sensitivity (Sen.), Specificity (Spec.), Accuracy (Acc.), Dice Similarity Coefficient (DSC), Overlap Measure (OM), Positive Predictive Value (PPV) and Root Mean Square Distance (RmsD):

$$Sen = \frac{TP}{TP + FN}\,, \tag{7}$$

$$Spec = \frac{TN}{FP + TN}\,, \tag{8}$$

$$Acc = \frac{TP + TN}{TP + TN + FP + FN}\,, \tag{9}$$

$$DSC = \frac{2 \times TP}{2 \times TP + FP + FN}\,, \tag{10}$$

$$OM = \frac{TP}{TP + FP + FN}\,, \tag{11}$$

$$PPV = \frac{TP}{TP + FP}\,, \tag{12}$$

$$RmsD = \sqrt{\frac{1}{M \times N} \sum_{y=1}^{N} \sum_{x=1}^{M} (R(x,y) - I(x,y))^2}\,, \tag{13}$$

where $R(x,y)$ is the gray value of the Ground Truth Image at (x,y) and $I(x,y)$ is the gray

Table 2. Performance Comparison between the existing method and the proposed method

	Using LIDC data		Using RIMS data	
	Existing Method	**Proposed Method**	**Existing Method**	**Proposed Method**
Accuracy (Acc)	0.98634	0.99958	0.99303	0.99805
Sensitivity (Sen)	0.92208	0.99759	0.96269	0.99204
Specificity (Spec)	1	1	0.99935	0.9993
Dice Similarity Coefficient (DSC)	0.95946	0.99879	0.97944	0.99433
Overlap Measure (OM)	0.92208	0.99759	0.9597	0.98872
Positive Predictive Value (PPV)	1	1	0.99677	0.99662
Root Mean Square Distance (RmsD)	0.11689	0.02057	0.08350	0.04419

value of the Segmented Image at (x, y).The performances of the proposed method are evaluated by using 10 CT scans of different patients from the Lung Image Database Consortium (LIDC) and another 10 CT scans collected from Regional Institute of Medical Sciences (RIMS), and then compared with that of the existing Image Thresholding Method [4] as shown in Table 2.

The graphs (shown in Figure 13 and 14) show the comparison between the proposed method and the existing threshold method in terms of sensitivity, specificity, and accuracy. From this graph, we found that the proposed method has higher sensitivity, specificity, and accuracy. Hence, the proposed method is more efficient than the existing Image Thresholding method.

5. Conclusion

The segmentation of lung including Juxta-Pleural nodule is a challenging task for many researches. The existing segmentation methods such as Image Thresholding, Region-growing algorithm, Active contour, Level sets, etc. fail to segment lungs including Juxta-Pleural nodules.

So, we proposed a new fully automated image processing method to segment lung including Juxta-Pleural nodules. The proposed method consists of two main stages: (i) Lung field extraction, which extracts initial lung region, and (ii) Boundary Analysis and Segmentation of Lung, which segments lungs with Juxta-Pleural nodules. And, we found the performance of the proposed method yields a better result than that of the existing Image Thresholding method [4].

The segmented lung obtains from the proposed system can further be applied to image processing steps (like Nodule Detection, Nodule Segmentation, and Nodule Diagnosis) in the CAD system for Lung Cancer. Hence, further works to detect, segment and diagnosis of lung cancer cells (pulmonary nodules), can be done efficiently from this proposed lung segmentation.

Acknowledgements

The authors acknowledge to all those who support directly or indirectly to complete this work, and also a special thank to *Dr. Gayatri Moirangthem* of Pathology Department (Regional Institute of Medical Sciences, Imphal) for her valuable suggestions.

References

1. **Cancer Facts & Figures. (2016)** *American Cancer Society's publication*. https://www.cancer.org/

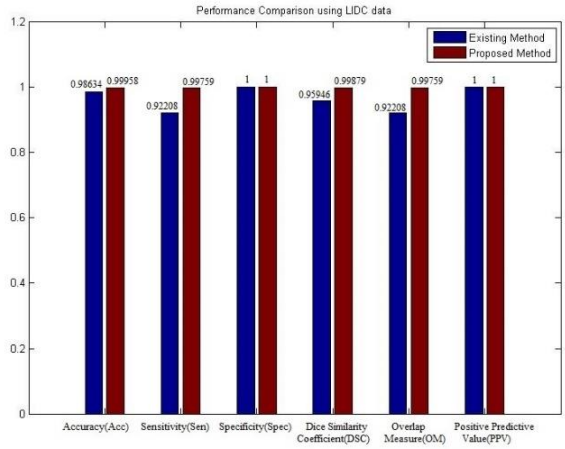

Fig. 13. Comparison between existing Image Thresholding method and the proposed method using LIDC data

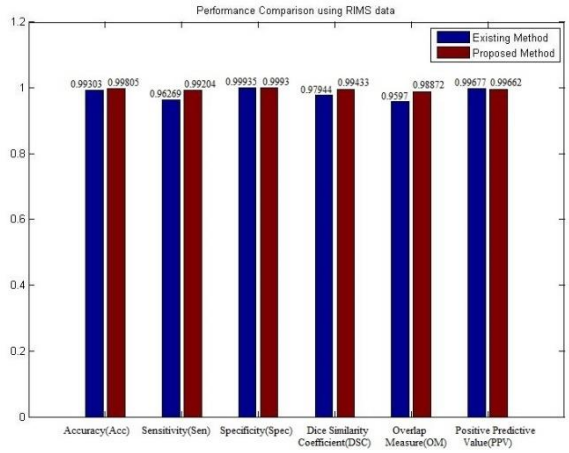

Fig. 14. Comparison between Image Thresholding method and the proposed method using RIMS data

content/dam/cancer-org/research/cancer-facts-and-statistics/annual-cancer-facts-and-figures/2017/cancer-facts-and-figures-2017.pdf. /accessed on 4th December, 2017.

2. **El-Baz, A., Beache, G.M., Gimel'farb, G., Suzuki, K., Okada, K., Elnakib, A., Soliman, A., & Abdollahi, B. (2013).** Computer-Aided Diagnosis Systems for Lung Cancer: Challenges and Methodologies. *International Journal of Biomedical Imaging,* Vol. 2013, pp. 46, DOI:101155/2013/942353.

3. **Armato III, S.G., McLennan, G., Bidaut, L., McNitt-Gray, M.F., Meyer, C.R., Reeves, A.P., Zhao, B., Aberle, D.R., Henschke, C.I., Hoffman, E.A., Kazerooni, E.A., MacMahon, H., vanBeek, E.J.R., Yankelevitz, D., & et al. (2011).** The Lung Image Database Consortium (LIDC) and Image Database Resource Initiative (IDRI): A completed reference database of lung nodules on CT scans. *Medical Physics*, Vol. 38, No. 2, pp. 915–931. DOI: 10.1118/1.3528204.

4. **Hu, S., Hoffman, E. A., & Reinhardt, J. M. (2001).** Automatic lung segmentation for accurate quantitation of volumetric X-ray CT images. *IEEE Transactions on Medical Imaging*, Vol. 20, No. 6, pp. 490–498. DOI: 10.1109/42.929615.

5. **Mendonca, A.M., da Silva, J.A. & Campilho, A. (2004).** Automatic delimitation of lung fields on chest radiographs. *Proceedings of the International Symposium on Biomedical Imaging (ISBI'04)*, Vol. 2, pp. 1287–1290. DOI:10.1109/ISBI.2004.1398781

6. **Yim, Y., Hong, H., & Shin, Y. G. (2005).** Hybrid lung segmentation in chest CT images for computer-aided diagnosis. *7th International Workshop on Enterprise Networking and Computing in Healthcare Industry, HEALTHCOM`05*, pp. 378–383. DOI: 10.1109/HEALTH.2005.1500486.

7. **Sluimer, I., Prokop, M., & Van-Ginneken, B. (2005).** Toward automated segmentation of the pathological lung in CT. *IEEE Transactions on Medical Imaging*, Vol. 24, No. 8, pp. 1025–1038. DOI: 10.1109/TMI.2005.851757.

8. **Campadelli, P., Casiraghi, E., & Artioli, D. (2006).** A fully automated method for lung nodule detection from postero-anterior chest radiographs. *IEEE Transactions on Medical Imaging*, Vol. 25, No. 12, pp. 1588–1603. DOI: 10.1109/TMI.2006.884198.

9. **Korfiatis, P., Skiadopoulos, S., Sakellaropoulos, P., Kalogeropoulou, C., & Costaridou, L. (2007).** Combining 2D wavelet edge highlighting and 3D thresholding for lung segmentation in thin-slice CT. *British Journal of Radiology*, Vol. 80, No. 960, pp. 996–1005. DOI: 10.1259/bjr/20861881.

10. **Gao, Q., Wang, S. J., Zhao, D., & Liu, L. (2007).** Accurate lung segmentation for X-ray CT images. *Proceedings of the 3rd International Conference on Natural Computation (ICNC '07)*, Vol. 2, pp. 275–279. DOI: 10.1109/ICNC.2007.157.

11. **Shi, Y., Qi, F., Xue, Z., & et al. (2008).** Segmenting lung fields in serial chest radiographs using both population-based and patient-specific shape statistics. *IEEE Transactions on Medical Imaging*, Vol. 27, No. 4, pp. 481–494. DOI:10.1109/TMI.2007.908130.

12. **El-Baz, A., Gimel'farb, G., Falk, R., Holland, T., & Shaffer, T. (2008).** A framework for unsupervised segmentation of lung tissues from low dose

computed tomography images. *Proceedings of the British Machine Vision Conference,* University of Leeds, UK, pp. 855–865.

13. **Annangi, P., Thiruvenkadam, S., Raja, A., Xu, H., Sun, X., & Mao, L. (2010).** Region based active contour method for x-ray lung segmentation using prior shape and low level features. *Proceedings of the 7th IEEE International Symposium on Biomedical Imaging: from Nano to Macro (ISBI '10),* pp. 892–895. DOI: 10.1109/ISBI.2010.5490130.
14. **Kockelkorn, T. T. J. P., Van-Rikxoort, E. M., Grutters, J. C., & Van-Ginneken, B. (2010).** Interactive lung segmentation in CT scans with severe abnormalities. *Proceedings of the 7th IEEE International Symposium on Biomedical Imaging: From Nano to Macro (ISBI '10)*, pp. 564–567. DOI:10.1109/ISBI.2010.5490285.
15. **Besbes, A. & Paragios, N. (2011).** Landmark-based segmentation of lungs while handling partial correspondences using sparse graph-based priors. *Proceedings of the International Symposium on Biomedical Imaging (ISBI '11)*, pp.989–995. DOI: 10.1109/ISBI.2011.5872568.
16. **Hua, P., Song, Q., Sonka, M., Hoffman, E. A., & Reinhardt, J. M. (2011).** Segmentation of pathological and diseased lung tissue in CT images using a graph-search algorithm. *Proceedings of the International Symposium on Biomedical Imaging (ISBI '11)*, pp. 2072–2075. DOI:10.1109/ISBI.2011.5872820.
17. **Sun, S., Bauer, C., & Beichel, R. (2012).** Automated 3-D segmentation of lungs with lung cancer in CT data using a novel robust active shape model approach. *IEEE Transactions on Medical Imaging,* Vol. 31, No. 2, pp. 449–460. DOI:10.1109/TMI.2011.2171357.
18. **Abdollahi, B., Soliman, A., Civelek, A. C. Li, X. F., Gimel'farb, G., & El-Baz, A. (2012).** A novel 3D joint MGRF framework for precise lung segmentation. *Proceedings of the MICCAI Workshop on Machine Learning in Medical Imaging, Nice,* pp.86–93. DOI:10.1007/978-3-642-35428-1_11.
19. **Gao, Q., Wang, S., Zhao, D., & Liu. J. (2007).** Accurate lung segmentation for X-ray CT images. *Proceedings of the 3rd International Conference on Natural Computation (ICNC '07)*, Vol. 2, pp. 275–279. DOI: 10.1109/ICNC.2007.157.
20. **Fisher, R., et al. (2003).** Connected Component Labeling. http:// homepages.inf. ed. ac. uk/rbf/HIPR2/label.htm. /accessed on 20th.
21. **Gonzalez, R. C. (2009).** *Digital image processing*. Pearson Education India.

Article received on 20/12/2016; accepted on 13/12/2017.
Corresponding author is Ratishchandra Huidrom.